Available online at www.sciencedirect.com
ScienceDirect
Ceramics International 37 (2011) 1549–1555
CERAMICS INTERNATIONAL
www.elsevier.com/locate/ceramint

Properties and consolidation of nanocrystalline WSi_2–SiC composite from mechanically activated powders by pulsed current activated combustion synthesis

In-Jin Shon [a,b,*], Jeong-Hwan Park [a,b], In-Yong Ko [a], Jung-Mann Doh [c], Jin-Kook Yoon [c], Kee-Seok Nam [d]

[a] Division of Advanced Materials Engineering, Research Center of Advanced Materials Development, Engineering College, Chonbuk National University, 664-14 Deokjin-dong 1-ga, Deokjin-gu, Jeonju, Jeonbuk 561-756, Republic of Korea
[b] Department of Hydrogen and Fuel Cells Engineering, Specialized Graduate School, Chonbuk National University, 664-14 Deokjin-dong 1-ga, Deokjin-gu, Jeonju, Jeonbuk 561-756, Republic of Korea
[c] Advanced Functional Materials Research Center, Korea Institute of Science and Technology, PO Box 131, Cheongryang, Seoul 130-650, Republic of Korea
[d] Korea Institute of Materials Science, 531 Changwondaero, Changwon, Gyeongnam 641-831, Republic of Korea

Received 1 February 2010; received in revised form 22 November 2010; accepted 12 January 2011
Available online 19 February 2011

Abstract

Dense nanostructured WSi_2–SiC composite was synthesized by pulsed current activated combustion synthesis method within 2 min in one step from mechanically activated powders of WC and 3Si. Simultaneous combustion synthesis and consolidation were accomplished under the combined effects of a pulsed current and mechanical pressure. Highly dense WSi_2–SiC with relative density of up to 99.8% was produced under simultaneous application of a 80 MPa pressure and the pulsed current. The average grain size and mechanical properties of the composite were investigated.

Keywords: C. Mechanical properties; Pulsed current activated combustion; Composite materials; Nanophase; WSi_2–SiC

1. Introduction

Interest in refractory metal silicides has increased significantly in recent years because of their potential application as high-temperature structural materials [1]. This class of materials has an attractive combination of properties, including high melting temperature, high modulus, high oxidation resistance in air, and a relatively low density [2,3]. Furthermore, the disilicides, in particular $TaSi_2$, $TiSi_2$, $MoSi_2$, $NbSi_2$, and WSi_2, have been used as Schottky barriers, ohmic contacts, gate materials, and interconnectors in integrated circuits, as a result of their low electrical resistivity, high stability, and good compatibility with silicon substrates [4,5].

However, as in the case of many intermetallic compounds, the current concern about these materials focuses on their low fracture toughness below the ductile–brittle transition temperature [6–9]. To improve on their mechanical properties, the approach commonly utilized has been the addition of a second phase to form composite [10–15] and to make nanostructured materials [16,17]. SiC is a very interesting ceramic material due to its properties like high hardness, low bulk density and high oxidation resistance which made SiC useful for a wide range of industrial application. Furthermore, the isothermal oxidation resistance of metal silicide–SiC composite in dry air was superior to that of monolithic metal silicide compact [18].

In recent days, nanocrystalline powders have been developed by the thermochemical and thermomechanical process named as the spray conversion process (SCP), co-precipitation and high energy milling [19–21]. However, the grain size in

* Corresponding author at: Division of Advanced Materials Engineering, Research Center of Advanced Materials Development, Engineering College, Chonbuk National University, 664-14 Deokjin-dong 1-ga, Deokjin-gu, Jeonju, Jeonbuk 561-756, Republic of Korea. Tel.: +82 63 270 2381; fax: +82 63 270 2386.
E-mail address: ijshon@chonbuk.ac.kr (I.-J. Shon).

0272-8842/$36.00
doi:10.1016/j.ceramint.2011.01.029

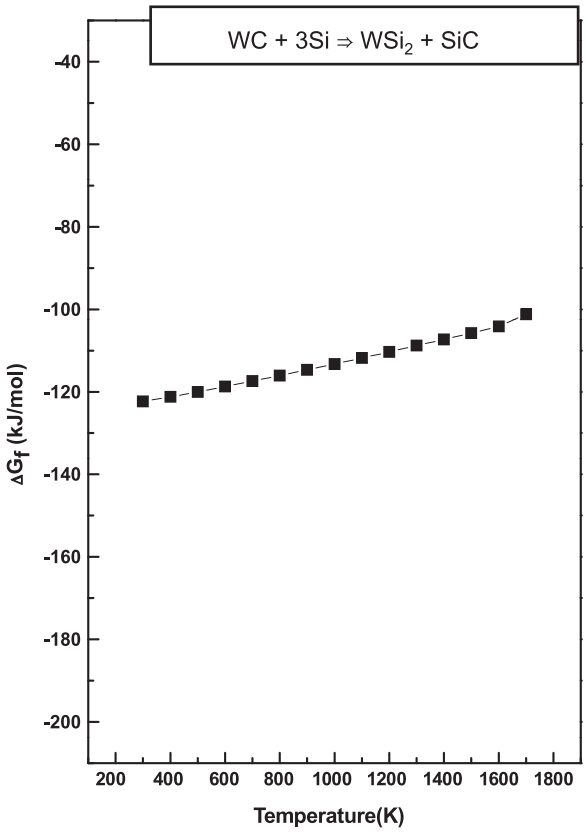

Fig. 1. Temperature dependence of the Gibbs free energy variation by interaction of tungsten carbide (WC) with silicon.

sintered materials becomes much larger than that in pre-sintered powders due to a fast grain growth during conventional sintering process. Therefore, even though the initial particle size is less than 100 nm, the grain size increases rapidly up to 500 nm or larger during the conventional sintering [22]. So, controlling grain growth during sintering is one of the keys to the commercial success of nanostructured materials. In this regard, the pulsed current activated sintering method which can make dense materials within 2 min, has been shown to be effective in achieving this goal [23,24].

It is apparently from Fig. 1 that when the WC phase is in contact with silicon, the formation of the WSi_2 and SiC phase can be thermodynamically possible by solid state displacement reaction according to following equation.

$$WC + 3Si \rightarrow WSi_2 + SiC \quad (1)$$

The purpose of this work is to produce dense nanocrystalline WSi_2–SiC composite within 2 min in one-step from mixtures of mechanically activated WC and 3Si powders by using this pulsed current activated combustion method and to evaluate its mechanical properties (hardness and fracture toughness).

2. Experimental procedures

Powders of 99.5% tungsten carbide (1.32 μm, TaeguTec Products) and 99% pure silicon (−325 mesh, Aldrich Products)

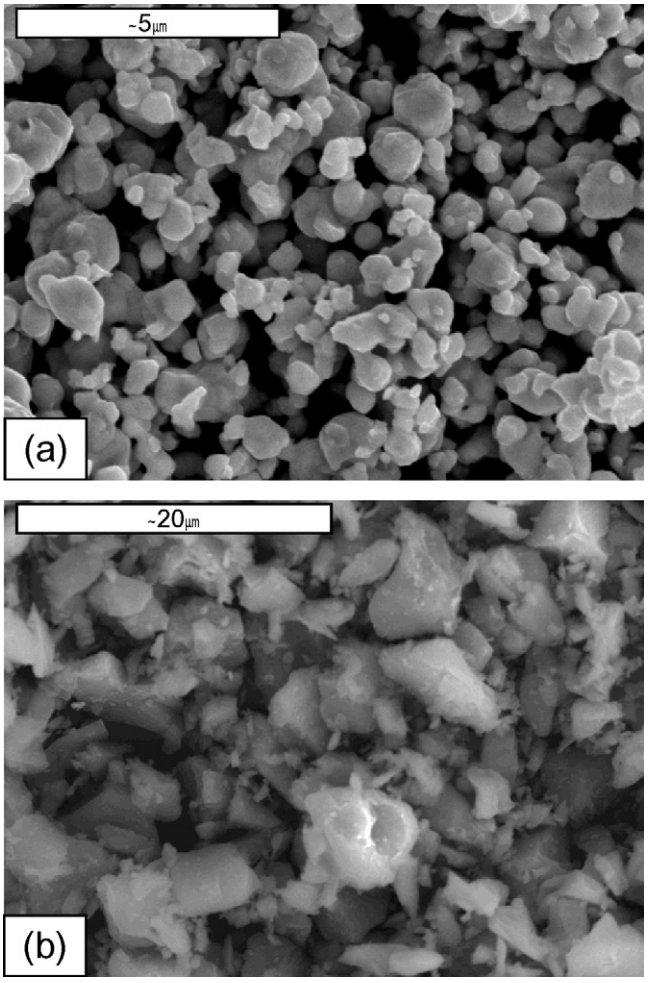

Fig. 2. Scanning electron microscope images of raw materials: (a) tungsten carbide and (b) silicon.

were used as a starting materials. Fig. 2 shows the SEM images of the raw materials used. WC and 3Si powder mixtures were first milled in a high-energy ball mill, Pulverisette-5 planetary mill with 250 rpm and for 10 h. Tungsten carbide balls (5 mm in diameter) were used in a sealed cylindrical stainless steel vial under argon atmosphere. The weight ratio of ball-to-powder was 30:1. The grain size and the internal strain were calculated by Suryanarayana and Norton's formula [25],

$$B_r(B_{\text{crystalline}} + B_{\text{strain}})\cos\theta = \frac{k\lambda}{L + \eta\sin\theta} \quad (2)$$

where B_r is the full width at half-maximum (FWHM) of the diffraction peak after instrument correction; $B_{\text{crystalline}}$ and B_{strain} are FWHM caused by small grain size and internal stress, respectively; k is constant (with a value of 0.9); λ is wavelength of the X-ray radiation; L and η are grain size and internal stress, respectively; and θ is the Bragg angle. The parameters B and B_r follow Cauchy's form with the relationship: $B = B_r + B_s$, where B and B_s are FWHM of the broadened Bragg peaks and the standard sample's Bragg peaks, respectively. Fig. 3 shows XRD patterns of the raw powders and the milled WC + 3Si powder mixture. The FWHM of the milled powder is greater than that of the raw powders due to internal

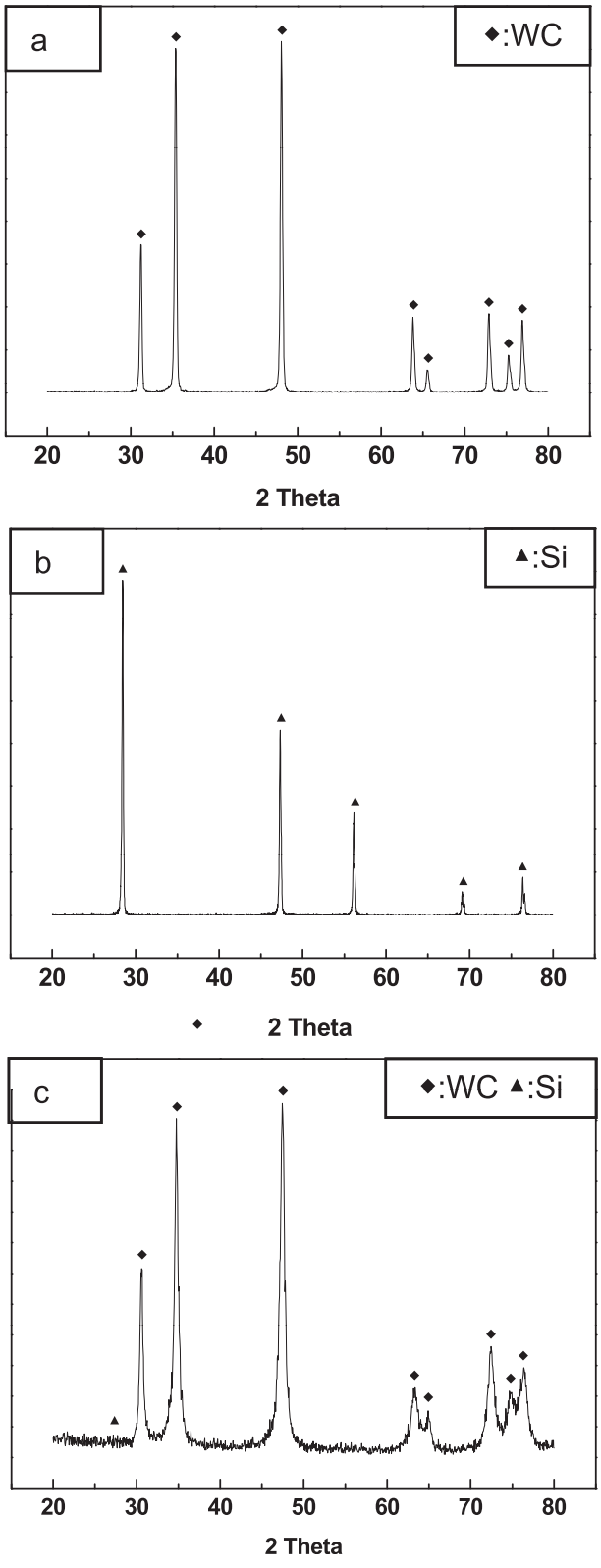

Fig. 3. XRD patterns of raw materials:(a) WC, (b) Si and (c) milled WC + 3Si.

strain and grain size reduction. The average grain sizes of the milled WC powders were determined as 20 nm.

After milling, the mixed powders were placed in a graphite die (outside diameter, 45 mm; inside diameter, 20 mm; height, 40 mm) and then introduced into the pulsed current activated

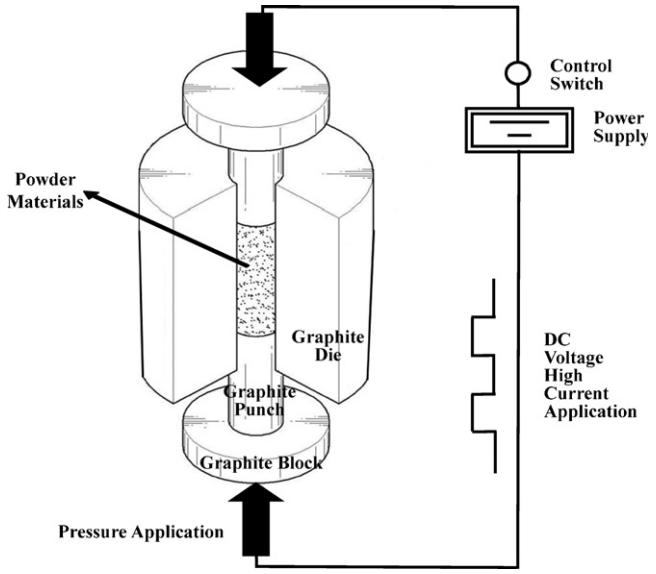

Fig. 4. Schematic diagram of the pulsed current activated combustion synthesis.

combustion system made by Eltek in South Korea, shown schematically in Fig. 4. The four major stages in the synthesis are as follows. The system was evacuated (stage 1). And a uniaxial pressure of 80 MPa was applied (stage 2). An induced current (frequency of about 50 kHz) was then activated and maintained until densification was attained as indicated by a linear gauge measuring the shrinkage of the sample (stage 3). Temperature was measured by a pyrometer which can detect temperature higher than 550 °C, focused on the surface of the graphite die. At the end of the process, the sample was cooled to room temperature (stage 4). The process was carried out under a vacuum of 40 mtorr.

The relative densities of the synthesized sample were measured by the Archimedes method. Microstructural information was obtained from product samples which were polished and etched using a solution of HF (10 vol.%), HNO_3 (30 vol.%) and H_2O (60 vol.%) for 3 min at room temperature. Compositional and micro structural analyses of the products were made through X-ray diffraction (XRD) and scanning electron microscopy (SEM) with energy dispersive X-ray analysis (EDAX). Vickers hardness was measured by performing indentations at load of 10 kg and a dwell time of 15 s on the synthesized samples.

3. Results and discussion

The variations in shrinkage displacement and temperature of the surface of the graphite die with heating time during the processing of WC + 3Si system are shown Fig. 5. As the pulsed current was applied the specimen showed initially a small (thermal) expansion and the shrinkage displacement increased gradually with temperature up to about 600 °C, but then abruptly increased at about 650 °C. When the reactant mixture of WC + 3Si was heated under 80 MPa pressure to 600 °C, no reaction took place and no significant shrinkage displacement

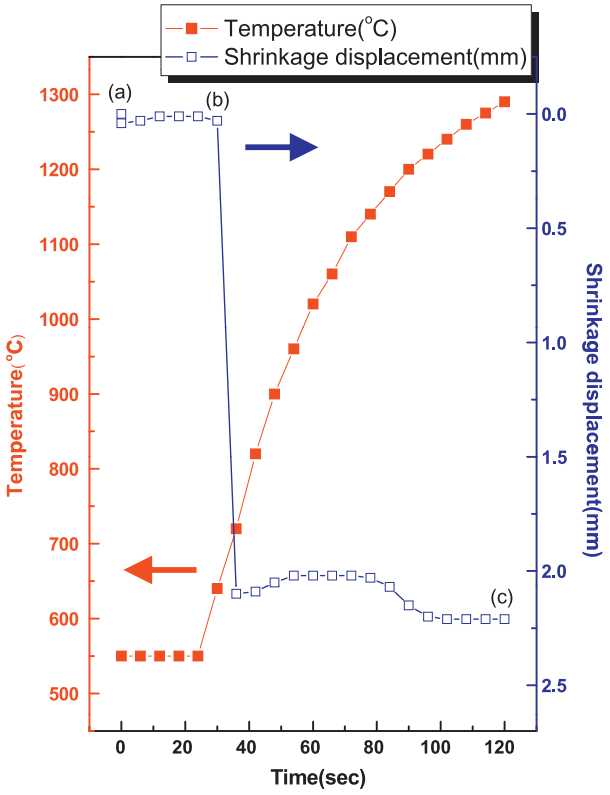

Fig. 5. Variation of temperature and shrinkage displacement with heating time during pulsed current activated combustion synthesis and densification of WSi_2–SiC (80 MPa, 2800 A).

as judged by subsequent XRD and SEM analyses. Fig. 6 shows the SEM (scanning electron microscope) image of a powder (a) after milling, a specimen (b) heated to 600 °C and (c) heated to 1280 °C, respectively. Fig. 6(a) and (b) indicates the presence of the reactants as separate phases. X-ray diffraction results, shown in Fig. 7 (a) and (b) exhibit only peaks pertaining to the reactants WC and Si. However, when the temperature was raised to 1280 °C, the starting powders reacted producing highly dense products. SEM image of an etched surface of the samples heated to 1280 °C under a pressure of 80 MPa is shown in Fig. 6(c). A complete reaction between these elements (WC and Si) has taken place under these conditions. These conclusions were supported by X-ray diffraction analyses with peaks of the product phase, WSi_2 and SiC phase, as indicated in Fig. 7(c). And minor phase (W_5Si_3) existed. The presence of W_5Si_3 of the sample suggests a deficiency of Si. It is considered that this observation is related to entrapped oxygen in the pores of the interior portion of the sample during pressing and may be due to a little oxidation of Si during the heating. There is low possibility of unreacted silicon because W compounds are thermodynamically more stable than silicon.

The abrupt increase in the shrinkage displacement at the ignition temperature is due to the increase in density as a result of molar volume change associated with the formation of WSi_2–SiC from WC + 3Si reactant and the consolidation of the product. In this study, the ignition temperature of WC + 3Si milled by high energy ball was about temperature of 650 °C. This temperature is lower than that of unmilled WC + 3Si

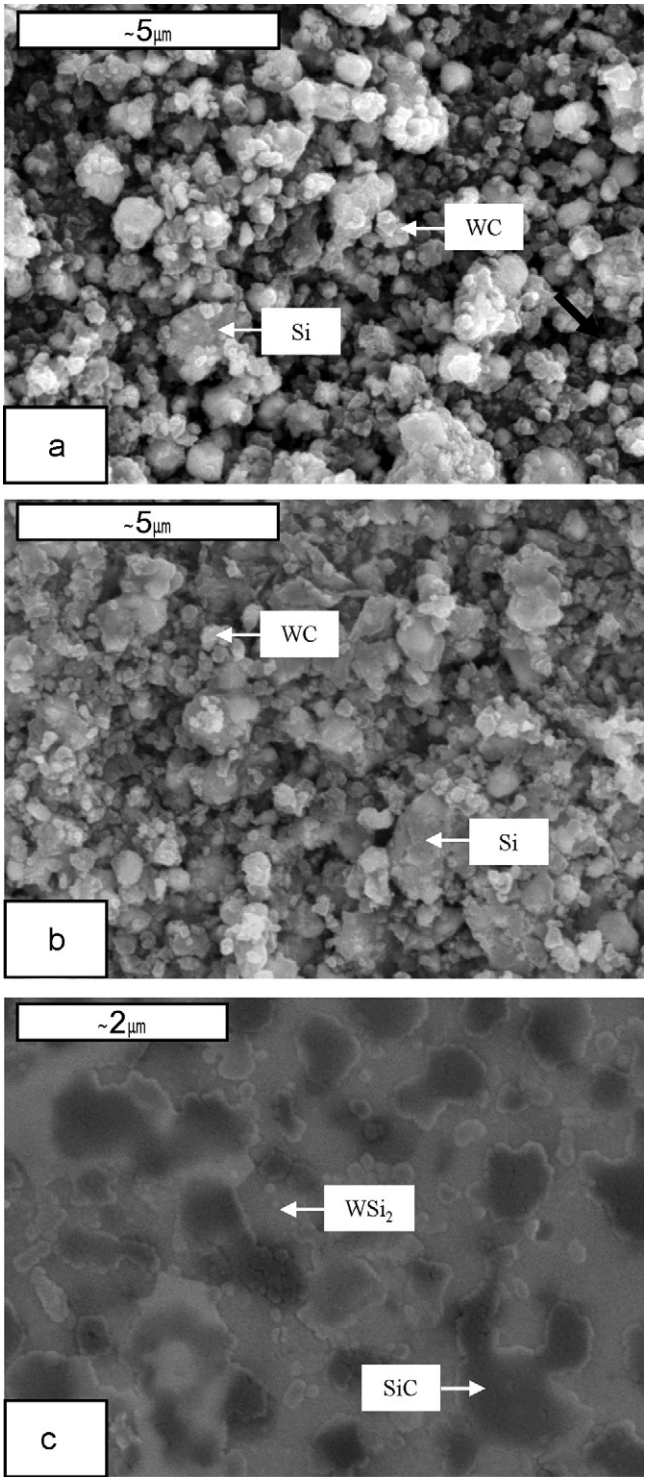

Fig. 6. Scanning electron microscope images of WC + 3Si system: (a) after milling, (b) before combustion synthesis, and (c) after combustion synthesis.

reported as about 1200 °C [26]. It is considered that milled powders reacts rapidly because refinement of powder by milling has many diffusion routes and activated state due to many defects and strain.

Fig. 8 shows plot of Br cos θ versus sin θ, indicating that the intercept ($K\lambda/L$) and slop (η) can be used to calculate the crystallite size and lattice strain (η). The structure parameters,

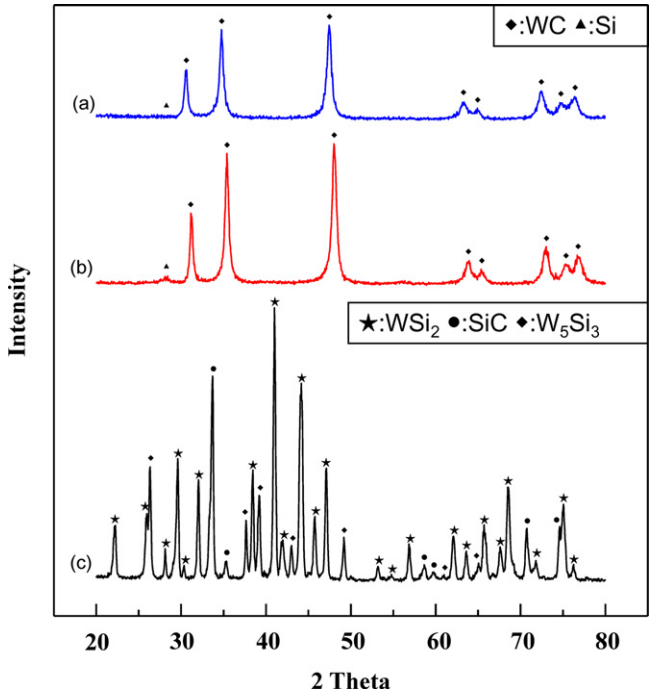

Fig. 7. XRD patterns of the WC + 3Si system: (a) after milling, (b) before combustion synthesis, and (c) after combustion synthesis.

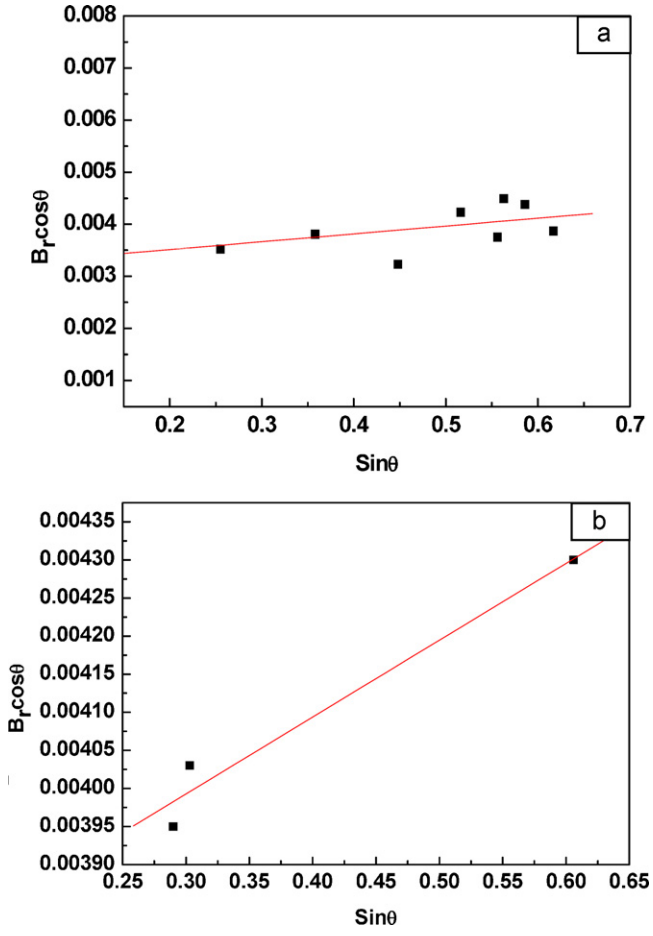

Fig. 8. Plot of Br cos θ versus sin θ for (a) WSi_2 and (b) SiC.

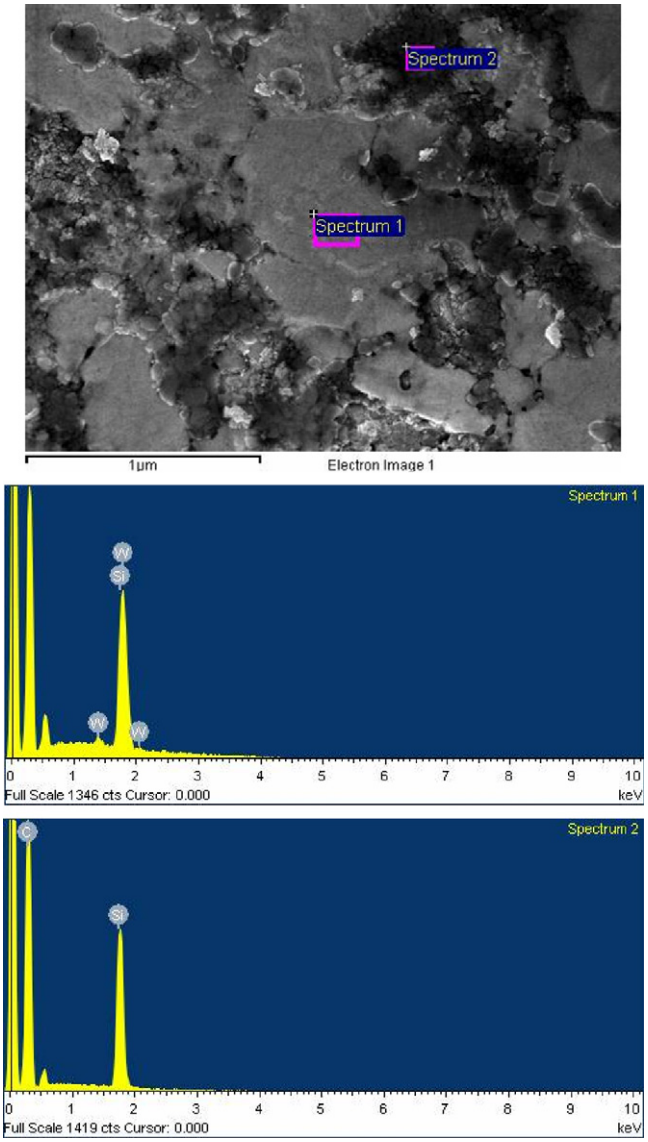

Fig. 9. FE-SEM image and EDS of WSi_2–SiC composite.

i.e. the average grain sizes of WSi_2 and SiC are obtained from by Suryanarayana and Norton's formula [25], were 47 nm and 38 nm, respectively and the SiC particles were well distributed in matrix, ascertained by SEM image of shown in Fig. 6(c). To confirm nanophase of WSi_2 and SiC, high resolution FE-SEM image and EDS analysis are shown in Fig. 9. The image consists of nanostructured WSi_2 (grey phase) and SiC (dark phase).

Vickers hardness measurements were made on polished sections of the WSi_2–SiC composite using a 10 kg load and 15 s dwell time. The calculated hardness value of WSi_2–SiC composite was 1698 kg/mm^2 which is higher than that of monolithic WSi_2 reported as 1375 kg/mm^2 [26] due to refinement of grain and addition of SiC. This value represents an average of five measurements. Indentations with large enough loads produced median cracks around the indent. The length of these cracks permits an estimation of the fracture toughness of the material by means of Anstis

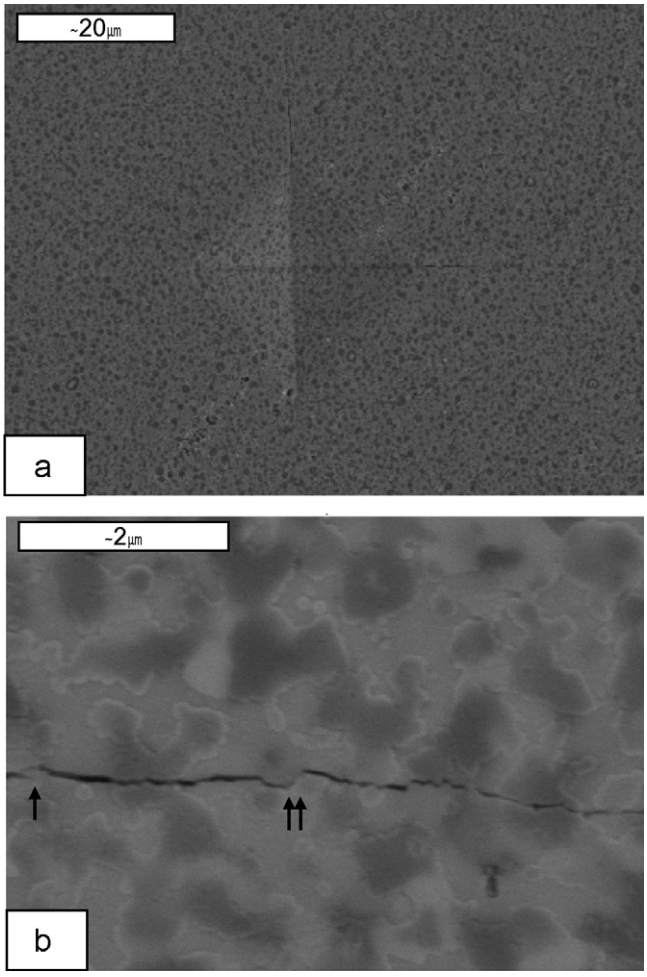

Fig. 10. (a) Vickers hardness indentation and (b) crack propagating of WSi_2–SiC composite.

expression [27].

$$K_{IC} = 0.016\left(\frac{E}{H}\right)^{1/2}\frac{P^{3/2}}{C} \quad (3)$$

where E is the Young's modulus, H is the indentation hardness, P is the indentation load, and C is the trace length of the crack measured from the center of the indentation. The modulus was estimated by the rule mixtures for the 0.327 volume fraction of SiC and the 0.673 volume fraction of WSi_2 using E(SiC) = 448 GPa [28] and E(WSi_2) = 467.9 GPa [29]. The calculated fracture toughness value of WSi_2–SiC composite is about 4.8 MPa $m^{1/2}$. The fracture toughness is higher than that of the SiC phases and WSi_2 phase reported as 1.8 MPa $m^{1/2}$ and 3.3 MPa $m^{1/2}$, respectively [9,26] due to crack deflection and branching shown in Fig. 10(b). As in the case of hardness value, the toughness value is the average of measurements on five measurements.

A typical indentation pattern for the WSi_2–SiC composite is shown in Fig. 10(a). Typically, one to three additional cracks were observed to propagate from the indentation corner. Higher magnification view of the indentation median crack in the WSi_2–SiC composite is shown in Fig. 10(b). The figure shows the crack deflection and crack branching.

Shon et al. [30] investigated simultaneous pulsed current activated combustion synthesis and densification of $NbSi_2$–SiC composite. The hardness (1698 kg/mm^2) of WSi_2–SiC composite is higher than that (1260 kg/mm^2) of $NbSi_2$-SiC composite because the hardness (1375 kg/mm^2) of WSi_2 is higher than that (876 kg/mm^2) of $NbSi_2$ [26,31]. These fracture toughnesses of the two composites are similar but higher than those monolithic phase due to addition of SiC.

4. Summary

Using the pulsed current activated combustion method, the simultaneous synthesis and densification of nanostructured WSi_2–SiC composite was accomplished from powders of WC and 3Si. Complete synthesis and densification can be achieved in one step within duration of 2 min. The relative density of the composite was 99.8% for the applied pressure of 80 MPa and the pulsed current. The average grain sizes of WSi_2 and SiC prepared by PCACS were about 47 nm and 38 nm, respectively. The average hardness and fracture toughness values obtained were 1698 kg/mm^2 and 4.8 MPa $m^{1/2}$, respectively. The present fracture toughness and hardness are higher than those of monolithic WSi_2.

Acknowledgement

This work was supported by National Research Foundation of Korea Grant funded by the Korean Government (2009-0065776).

References

[1] N.S. Stoloff, Mater. Sci. Eng. A 261 (1999) 169–180.
[2] A.K. Vasudevan, J.J. Petrovic, Mater. Sci. Eng. A 155 (1992) 259–266.
[3] G.J. Fan, M.X. Quan, Z.Q. Hu, J. Eckert, L. Schulz, Scripta Mater. 41 (1999) 1147–1151.
[4] M.E. Schlesinger, Chem. Rev. 90 (1990) 607–628.
[5] A.K. Vasudevan, J.J. Petrovic, Mater. Sci. Eng. A 155 (1992) 1–17.
[6] J. Li, D. Jiang, S. Tan, J. Eur. Ceram. Soc. 20 (2000) 227–233.
[7] G. Sauthoff, Intermetallics, VCH Publishers, New York, 1995.
[8] Y. Ohya, M.J. Hoffmann, G. Petzow, J. Mater. Sci. Lett. 12 (1993) 149–152.
[9] J. Qian, L.L. Daemen, Y. Zhao, Diam. Relat. Mater. 14 (2005) 1669–1672.
[10] B.W. Lin, T. Iseki, Br. Ceram. Trans. J. 90 (1992) 1–5.
[11] Y. Ohya, M.J. Hoffmann, G. Petzow, J. Am. Ceram. Soc. 75 (1992) 2479–2483.
[12] S.K. Bhaumik, C. Divakar, A.K. Singh, G.S. Upadhyaya, Mater. Sci. Eng. A 279 (2000) 275–281.
[13] D.K. Jang, R. Abbaschian, Korean J. Mater. Res. 9 (1999) 92–98.
[14] H. Zhang, P. Chen, M. Wang, X. Liu, Rare Metals 21 (2002) 304–307.
[15] D.Y. Oh, H.C. Kim, J.K. Yoon, I.J. Shon, J. Alloys Compd. 395 (2005) 174–180.
[16] M. Sherif El-Eskandarany, J. Alloys Compd. 305 (2000) 225–238.
[17] L. Fua, L.H. Caob, Y.S. Fan, Scripta Mater. 44 (2001) 1061–1068.
[18] J.K. Yoon, K.H. Lee, G.H. Kim, J.H. Han, J.M. Doh, K.T. Hong, Mater. Trans. 45 (2004) 2435–2442.
[19] Z. Fang, J.W. Eason, Int. J. Refract. Met. Hard Mater. 13 (1995) 297–303.
[20] I.J. Shon, D.K. Kim, K.T. Lee, K.S. Nam, Met. Mater. Int. 14 (2008) 593–598.
[21] B.R. Kim, K.D. Woo, J.K. Yoon, J.M. Doh, I.J. Shon, J. Alloys Compd. 481 (2009) 573–576.

[22] M. Sommer, W.D. Schubert, E. Zobetz, P. Warbichler, Int. J. Refract. Met. Hard Mater. 20 (2002) 41–50.
[23] H.C. Kim, I.J. Shon, J.K. Yoon, J.M. Doh, Int. J. Refract. Met. Hard Mater. 25 (2007) 46–52.
[24] I.J. Shon, S.C. Kim, B.S. Lee, B.R. Kim, Electron. Mater. Lett. 5 (2009) 19–22.
[25] C. Suryanarayana, M.G. Norton, X-ray Diffraction A Practical Approach, Plenum Press, New York, 1998.
[26] D.Y. Oh, H.C. Kim, J.K. Yoon, I.Y. Ko, I.J. Shon, Met. Mater. Int. 12 (2006) 307–315.
[27] G.R. Anstis, P. Chantikul, B.R. Lawn, D.B. Marshall, J. Am. Ceram. Soc. 64 (1981) 533–538.
[28] F. Monteverde, Comp. Sci. Technol. 65 (2005) 1869–1879.
[29] F. Chu, M. Lei, S.A. Maloy, J.J. Petrovic, T.E. Mitchell, Acta Mater. 44 (1996) 3035–3048.
[30] I.J. Shon, H.k. Park, H.C. Kim, J.K. Yoon, I.Y. Ko, Ceram. Int. 34 (2008) 615–619.
[31] I.Y. Ko, B.R. Kim, K.S. Nam, B.M. M, B.S. Lee, I.J. Shon, Met. Mater. Int. 15 (2009) 399–403.